DIGITAL ACCESS TO SCHOLARSHIP AT HARVARD
DASH.HARVARD.EDU

HARVARD LIBRARY

Uba1 functions in Atg7- and Atg3-independent autophagy

Citation

Chang, Tsun-Kai, Bhupendra V. Shravage, Sebastian D. Hayes, Christine M. Powers, Rachel T. Simin, J. Wade Harper, and Eric H. Baehrecke. 2013. “Uba1 functions in Atg7- and Atg3-independent autophagy.” Nature cell biology 15 (9): 1067-1078. doi:10.1038/ncb2804. http://dx.doi.org/10.1038/ncb2804.

Published version

https://doi.org/10.1038/ncb2804

Link

http://nrs.harvard.edu/urn-3:HUL.InstRepos:12064440

Terms of use

This article was downloaded from Harvard University’s DASH repository, and is made available under the terms and conditions applicable to Other Posted Material (LAA), as set forth at

https://harvardwiki.atlassian.net/wiki/external/NGY5NDE4ZjgzNTc5NDQzMGIzZWZhMGFlOWI2M2EwYTg

Accessibility

https://accessibility.huit.harvard.edu/digital-accessibility-policy

Share Your Story

The Harvard community has made this article openly available.
Please share how this access benefits you. Submit a story

NIH Public Access
Author Manuscript
Nat Cell Biol. Author manuscript; available in PMC 2014 March 01.

Published in final edited form as:
Nat Cell Biol. 2013 September ; 15(9): 1067–1078. doi:10.1038/ncb2804.

Uba1 functions in Atg7- and Atg3-independent autophagy

Tsun-Kai Chang[1], **Bhupendra V. Shravage**[1], **Sebastian D. Hayes**[2], **Christine M. Powers**[1], **Rachel T. Simin**[1], **J. Wade Harper**[2], and **Eric H. Baehrecke**[1,3]

[1]Department of Cancer Biology, University of Massachusetts Medical School, Worcester, MA 01605 USA

[2]Department of Cell Biology, Harvard Medical School, Boston, MA 02115 USA

Abstract

Autophagy is a conserved process that delivers components of the cytoplasm to lysosomes for degradation. The E1 and E2 enzymes encoded by *Atg7* and *Atg3* are thought to be essential for autophagy involving the ubiquitin-like protein Atg8. Here, we describe an Atg7- and Atg3-independent autophagy pathway that facilitates programmed reduction of cell size during intestine cell death. Although multiple components of the core autophagy pathways, including Atg8, are required for autophagy and cells to shrink in the midgut of the intestine, loss of either Atg7 or Atg3 function does not influence these cellular processes. Rather, Uba1, the E1 used in ubiquitination, is required for autophagy and reduction of cell size. Our data reveal that distinct autophagy programs are used by different cells within an animal, and disclose an unappreciated role for ubiquitin activation in autophagy.

INTRODUCTION

Macroautophagy (autophagy) is a system that is used to transfer cytoplasmic material, including proteins and organelles, to lysosomes by all eukaryotic cells [1]. Autophagy is augmented during cell stress to reduce damage to enable cell survival, and is also associated with the death of animal cells [2, 3]. Although most studies of this process have focused on stress-induced autophagy, such as nutrient deprivation, autophagy is also a normal aspect of animal development where it is required for proper death and removal of cells and tissues [4-6]. Defects in autophagy lead to accumulation of protein aggregates and damaged organelles, as well as human disorders [1, 7]. Most of our knowledge about the genes controlling autophagy is based on pioneering studies in the yeast *Saccharomyces cerevisiae* [8] - [11], and it is not clear if cells that exist in extremely different contexts within multi-cellular organisms could use alternative factors to regulate this catabolic process.

Atg genes that are conserved from yeast to humans are required for autophagy, and include the Atg1 and Vps34 regulatory complexes, as well as two ubiquitin-like conjugation pathways [1]. The two ubiquitin-like molecules, named Atg8 (LC3/GABARAP in mammals) and Atg12, become associated with the isolation membranes that form autophagosomes through the activity of the E1 enzyme Atg7. Atg3 functions as the E2 conjugating enzyme for Atg8, while Atg10 functions as the E2 for Atg12 [12]. Atg12 associates with Atg5 and

[3]Correspondence should be addressed to E.H.B. (Eric.Baehrecke@umassmed.edu) .

AUTOHR CONTRIBUTIONS

T.-K.C., B.V.S., S.D.H., J.W.H., and E.H.B. designed the experiments. All experiments were performed by T.-K.C., except Fig. 4d,e by B.V.S., TEM by T.-K.C., B.V.S., C. M. P., and R.T.S. and E1 charging assays by S.D.H.. T.-K.C., B.V.S. and E.H.B. wrote the manuscript and all authors commented on it.

Note: Supplementary Information is available in the online version.

NIH-PA Author Manuscript
NIH-PA Author Manuscript
NIH-PA Author Manuscript

NIH-PA Author Manuscript

NIH-PA Author Manuscript

NIH-PA Author Manuscript

Atg16 during the formation of the autophagosome, and Atg8 is conjugated to the lipid phosphatidyl-ethanolamine enabling this protein to associate with the isolation membrane and autophagosome. Lipidated Atg8 remains associated with autophagosomes until fusion with lysosomes to form autolysosomes where cargos are degraded by lysosomal enzymes.

Degradation of the midgut of the *Drosophila* intestine involves a large change in midgut length, has elevated autophagy and markers of caspases associated with it, requires autophagy, and appears to be caspase-independent [13-15]. Here, we show that autophagy is required for programmed reduction in cell size at the onset of intestine cell death in *Drosophila. Atg* genes encoding components of the Atg1 and Vps34 complexes are required for midgut cell autophagy and reduction in size. Surprisingly, although Atg8a is required for autophagy and programmed cell size reduction, the evolutionarily conserved E1 activating enzyme Atg7 and E2 conjugating enzyme Atg3 are not required for these cellular events. We screened the E1 activating enzymes encoded by the fly genome and identified *Uba1* as being required for autophagy and reduction of cell size during midgut cell death. Although the genes that control autophagy are conserved throughout eukaryotes, our data provide evidence indicating that the core autophagy machinery may not be identical in all cells within an organism.

RESULTS

Autophagy is required for programmed cell size reduction during cell death

The dying *Drosophila* larval intestine undergoes a dramatic reduction in midgut length at the onset of puparium formation [14, 15], and this change in structure requires autophagy and appears to be caspase-independent [13]. We investigated the morphology of midgut cells in order to gain insight into how autophagy may contribute to the dramatic change in larval intestine structure. We noticed that wild-type, as well as *Atg18*/wild-type and *Atg2*/wild-type heterozygous control, midgut cells undergo a dramatic reduction in size following the induction of autophagy from the third instar larval stage to pre-pupal stage (Fig. 1a-f). By contrast, *Atg18/Df* and *Atg2/Df* mutant animals lacked autophagy in the midgut based on transmission electron microscopy (TEM) (Fig. 1g-j) and GFP-Atg8a reporter analyses [13]. Moreover, we observed double membrane autophagosomes containing either mitochondria or ribosomes in control midgut cells (enlarged images in Fig. 1g,i). Significantly, either *Atg18/Df* or *Atg2/Df* mutant midguts showed a remarkable inhibition of the decrease in cell size (Fig. 1c-f). Thus, the striking reduction in midgut cell size involves a programmed process requiring autophagy.

We tested if the requirement of *Atg* genes for cell size reduction is cell autonomous by expression of a double-stranded inverse-repeat (IR) construct designed to target and knockdown *Atg18* ($Atg18^{IR}$) in clones of cells. Indeed, cells expressing $Atg18^{IR}$ were significantly larger than neighboring cells (Fig. 2a,b). Furthermore, cells that expressed $Atg18^{IR}$ exhibited attenuated autophagy; compared to smaller neighboring cells, they possessed far fewer autophagosomes based on the detection of mCherry-Atg8a puncta (Fig. 2c). In addition, either a loss-of-function mutation in *Atg1* or knockdown of *Atg1* prevented cells from shrinking (Fig. 2d-f). Importantly, knockdown of *Atg1* in clones of cells also attenuated the formation of mCherry-Atg8a puncta compared to the smaller neighboring control cells (Fig. 2f). Moreover, reduced *Atg1* function does not influence midgut cell size in third instar larvae (Supplementary Fig. S1a,b), further indicating that loss of autophagy does not influence cell growth during early development and that autophagy is required for cells to decrease in volume at the end of larval development. We investigated if analyses of cell size reflect a similar change in midgut cell volume (Fig. 2g-k), and determined that 2-dimensional measurements of cell size accurately represent the changes observed in

NIH-PA Author Manuscript

NIH-PA Author Manuscript

NIH-PA Author Manuscript

shrinking midgut cells. These data indicate that autophagy is required in a cell autonomous manner for the programmed reduction of midgut cell size at the end of larval development.

To test whether other autophagy genes are required for midgut cells to shrink, we altered the function of multiple *Atg* genes in clones of midgut cells. *Vps34, Atg8a, Atg12, Atg13, Atg6, Atg5*, and *Atg16* (*CG31033*) were each required for programmed size reduction of midgut cells (Fig. 3a-f and Supplementary Fig. S1c-j). By contrast, expression of the caspase inhibitor p35 in clones of midgut cells did not influence cell size (Supplementary Fig. S1k,l). These data indicate that autophagy, but not caspase activation, is required for *Drosophila* midgut degradation during animal development.

Mis-expression of Atg1 is sufficient to induce autophagy in multiple *Drosophila* cell types [4, 16]. Similarly, Atg1 mis-expression in clones of early third instar larval midgut cells was sufficient to induce premature autophagy and decreased the size of these cells (Fig. 3g,g'). Importantly, knockdown of *Atg8a* suppressed Atg1-induced cells from shrinking (Fig. 3h), indicating that the sufficiency for Atg1 to induce premature cell shrinking depends on core autophagy gene function. Surprisingly, however, knockdown of *Atg7* failed to suppress the Atg1-induced autophagy and reduction in cell size phenotypes (Fig. 3i,i') even though the same *Atg7* knockdown strain suppresses starvation-induced autophagy in the fat body (Supplementary Fig. S2a). Our results indicate that many of the core autophagy genes that are conserved between yeast and humans are required for autophagy and cell size reduction during larval midgut cell death, and this process appears to be independent of *Atg7*.

Programmed cell size reduction, autophagy and clearance of mitochondria are Atg7-independent

Atg7 encodes an evolutionarily conserved E1 activating enzyme that is required for autophagy in all organisms and cell types that involve Atg8/LC3 that have been previously studied [1, 12]. Unlike several other genes that are required for autophagy in *Drosophila*, loss of *Atg7* fails to cause animal lethality, and previous studies indicate that *Atg7* mutations inhibit autophagy in the fly midgut [17]. This previous study analyzed autophagy in midguts of third instar larvae when autophagy is relatively low and variable. These results, combined with our observation that *Atg7* knockdown failed to suppress Atg1-induced decrease in cell size, prompted us to revisit the role of *Atg7* in midgut autophagy in greater detail. As reported previously [17], mutant clones of $Atg7^{d4}$ cells failed to induce autophagy under nutrient deprivation in larval fat body cells (Supplementary Fig. S2b). By contrast, $Atg7^{d4}$ mutant clones of midgut cells, as well as *Atg7* knockdown midgut cells, possessed autophagy and underwent normal reductions in cell size (Fig. 4a-c and Supplementary Fig. S2c,d). In addition, GFP-Atg8a puncta formation is similar in control and null loss of *Atg7* function mutant midgut cells (Fig. 4d,e). Furthermore, loss of *Atg7* did not influence the formation of GFP-Atg5 puncta (Fig. 4f) which depended on the function of *Vps34* (Supplementary Fig. S2e). We used TEM to analyze control and *Atg7* null mutant midguts, and found that autophagosomes and autolysosomes were present even in the absence of *Atg7* function (Fig. 4g, h). Significantly, we observed cytoplasmic material, including mitochondria and ribosomes, in double membrane autophagosomes in *Atg7* mutant cells (enlarged image in Fig. 4h). These results indicate that *Atg7* is not required for autophagy and for cells to shrink in the midgut.

The presence of cytoplasmic material in the autophagosomes of *Atg7* null intestine cells prompted us to investigate if *Atg* genes are required for mitochondria clearance (mitophagy). We quantified the number of mitochondria in control, *Atg18* mutant, and *Atg7* mutant cells, and discovered that *Atg18* mutant cells, but not *Atg7* mutant cells, had more mitochondria than control midgut cells (Fig. 5a). Homozygous *Atg1* mutant clone and

NIH-PA Author Manuscript

NIH-PA Author Manuscript

NIH-PA Author Manuscript

neighboring control cells possessed similar amounts GFP-labeled mitochondria before the onset of autophagy in the intestines of third instar larvae (Fig. 5b), indicating that loss of Atg1 does not dramatically alter mitochondria numbers during development. By contrast, we observed significant retention of GFP-labeled mitochondria in homozygous *Atg1* mutant intestine cells compared to their control neighbors following the onset of autophagy (Fig. 5c). Combined, these data indicate that most autophagy genes, but not *Atg7*, are required for cell size reduction, clearance of cytoplasmic material, and autophagy.

Uba1 is required for autophagy and cell size reduction

The lack of *Atg7* function in midgut cell autophagy and shrinking prompted us to screen for other Ubiquitin-like activating enzymes (Ubas) that are required for autophagy and midgut cells to decrease in size. Six predicted Ubas are encoded in the *Drosophila* genome, termed *Uba1* (CG1728), *Uba2* (CG7528), CG13343 (human *Uba3* homolog), CG13090 (*Uba4* homolog), CG1749 (*Uba5* homolog) and *Atg7*. We expressed RNAi knockdown transgenes against all of the Ubas, as well as *Aos1* (CG12276, *Uba2* binding partner) and *APP-BP1* (CG7828, CG13343 binding partner), in clones of midgut cells, and *Uba1* was the only gene that exhibited a defect in cell size reduction (Fig. 6a,b and Supplementary Fig. S3). Both midgut cell size reduction and autophagy were inhibited when *Uba1* was knocked down (Fig. 6a,b and Supplementary Fig. S4a). Consistent with this conclusion, *Uba1* knockdown did not alter cell growth during larval development (Supplementary Fig. S4b,c). Similar defects in the reduction in midgut cell size were observed when *Uba1* function was reduced in clones of cells using the temperature sensitive mutant $Uba1^{H33}$ (Fig. 6c,d), thus demonstrating a cell-autonomous role for Uba1 in midgut cell size reduction. Clones of $Uba1^{H33}$ cells also showed reduced Atg8a puncta, reduced Atg5 puncta, and accumulation of p62/Ref(2)P proteins (Fig. 6e-g), further demonstrating that Uba1 is required for midgut autophagy and programmed size reduction.

Uba1 activates ubiquitin and transfers it to a family of E2 conjugating enzymes, which then transfer ubiquitin to substrates via an E3 ubiquitin ligase. Protein carrying lysine-48 linked poly-ubiquitin chains are targeted to the proteasome for degradation. To determine if midgut cell shrinking was influenced by altered proteasome function, we expressed *Dts7*, a dominant temperature sensitive mutant of the β2 subunit of the proteasome [18], in clones of cells in the midgut. We also monitored the activity of the proteasome using CL1-GFP as a reporter [19]. When proteasome function was impaired by mis-expression of dominant proteasome subunit mutant *Dts7* in clones of cells, CL1-GFP was retained, and midgut cells underwent normal reductions in cell volume (Fig. 6h,i and Supplementary Fig. S4d). These data indicate that the function of the proteasome is not required for programmed reduction of midgut cell size.

We tested if *Uba1* is required for autophagy that is induced by stress in different tissues. Decreased *Uba1* function did not influence starvation-induced autophagy in either the fat body or midgut (Supplementary Fig. S5a-d). In addition, knockdown of *Uba1* did not alter hydrogen peroxide-triggered autophagy in the midgut (Supplementary Fig. S5e,f).

Uba1 could regulate autophagy by multiple possible mechanisms. One possibility is that Uba1 functions as the E1 enzyme in place of Atg7 to control the lipidation of Atg8. To test this possibility, we performed an *in vitro* E1 charging assay using Uba1 and Atg7 as E1s to be charged with either Atg8a or ubiquitin (Ub). As expected, Uba1 and Atg7 were charged with ubiquitin and Atg8a, respectively, and these thioester bonds were reversed by the addition of reducing agent (Fig. 7a,b and Supplementary Fig. S6a,b). By contrast, Uba1 was unable to activate Atg8a and Atg7 was unable to activate ubiquitin (Fig. 7a,b). These data suggest that Uba1 does not substitute for Atg7 as the E1 for Atg8a conjugation.

NIH-PA Author Manuscript

NIH-PA Author Manuscript

NIH-PA Author Manuscript

Most autophagy genes that we tested are required for the formation of *Atg8a* puncta and programmed cell size reduction in the midgut cells of intestines (Fig. 1-3, Supplementary Fig. S1), but *Atg7* is not needed for these cellular changes (Fig. 4). Since Atg8a puncta formation is thought to always depend on conjugation of phosphatidyl-ethanolamine, we tested whether Atg8a lipidation occurs in *Atg7* mutant intestines. Protein extracts from midguts of wild-type control, *Atg7* mutant and *Atg8a* mutant animals at puparium formation were subjected to immunoblot analysis using Atg8a antibody. Small amounts of lipidated Atg8a (Atg8a-II) were detected in wild-type midgut extracts, but not in either *Atg7* or *Atg8a* mutant midguts (Fig. 7c), indicating that *Atg7* is indeed essential for Atg8 lipidation.

Since *Atg7* mutant midgut cells exhibited normal autophagy (Fig. 4), we hypothesized that Atg8 lipidation is not required for midgut autophagy and programmed cell size reduction. This hypothesis would predict that *Atg3*, the E2 conjugating enzyme for Atg8 lipidation, is also not required for midgut autophagy. Although *Atg3* is required for starvation-induced autophagy in *Drosophila* fatbody [16], *Atg3* null mutant midgut cells exhibited normal size reduction and autophagy (Fig. 7d,e and Supplementary Fig. S6c,d). Moreover, knockdown of *Atg3* showed similar phenotype as knockdown of *Atg7*; although Atg3 was required for autophagy in starved fatbody, knockdown of *Atg3* did not suppress Atg1-induced reduction in midgut cell size (Fig. 7f, Supplementary Fig. S6e).

The cysteine protease Atg4 is required for processing of Atg8/LC3 so that it can be conjugated to phosphatidyl-ethanolamine, as well as for de-lipidation of Atg8/LC3 at a later stage in autophagy. A dominant negative form of human Atg4B was shown to inhibit LC3 lipidation and autophagy [20], and a similar dominant negative form of Atg4a was shown to inhibit autophagy in *Drosophila* [21]. To further test the requirement for Atg8a lipidation in midgut cell size reduction, we expressed dominant negative Atg4 ($Atg4^{DN}$). Consistent with our other results, expression of $Atg4^{DN}$ in clones of cells did not alter their reduction in size (Fig. 7g,h). Combined, these data suggest that Atg8a lipidation, as well as the E1 and E2 enzymes Atg7 and Atg3, are not required for midgut autophagy.

Our data indicate that Uba1 does not substitute for Atg7. Therefore, we investigated alternative explanations for how Uba1 regulates autophagy and cell size reduction in the dying midgut of *Drosophila*. A rise in steroid hormone triggers the induction of caspases and autophagy that precede midgut cell death [13, 14, 22], and it is possible that Uba1 influences all of these pathways. The steroid-regulated primary response protein BrC was present in *Uba1* knockdown cells even though cell size reduction was inhibited (Supplementary Fig. S6f), indicating that Uba1 does not influence global aspects of steroid signaling. In addition, *Uba1* knockdown did not influence the expression of the steroid-regulated pro-apoptotic factor Hid (Supplementary Fig. S6g). Combined, these data suggest the possibility that Uba1 may function directly in regulating autophagy. Although previous studies have suggested that receptors that bind to ubiquitinated cargo play an important role in early stages of autophagy [23, 24], no study has directly implicated ubiquitination as a key regulatory step in autophagosome formation. Therefore, such a model would predict that ubiquitin is required for autophagy and cell size reduction. We tested this model by knockdown of ubiquitin in clones of midgut cells, and saw that ubiquitin was required for Atg8a puncta formation (Fig. 7i) and programmed cell size reduction in the midgut (Fig. 7j,k). Significantly, the Atg1-induced small cell size phenotype (Fig. 7l) was suppressed when *Uba1* function was reduced (Fig. 7m,n). These data indicate that *Uba1* functions downstream of Atg1-regulated autophagy.

Midgut cells accumulate p62 and fail to form both Atg8a and Atg5 puncta when *Uba1* function is reduced (Fig. 6e-g). To determine if this E1 is required for removal of cytoplasmic material, we investigated the clearance of mitochondria from the cytoplasm of

NIH-PA Author Manuscript

NIH-PA Author Manuscript

NIH-PA Author Manuscript

cells with decreased *Uba1* function. Homozygous *Uba1* mutant and neighboring control cells possessed similar amounts GFP-labeled mitochondria before the onset of autophagy in the intestines of third instar larvae (Fig. 8a). These data indicate that reduced *Uba1* function does not dramatically alter mitochondria numbers during development. Significantly, we observed retention of both GFP-labeled mitochondria and mitochondrial ATP synthase complex V (ATPV) in intestine cells with reduced *Uba1* function compared to their control neighbors following the onset of autophagy (Fig. 8b,c). We then performed immuno-TEM to identify *Uba1* knockdown cells that express both $Uba1^{IR}$ and GFP. Control cells lacking immuno-labeled gold particles possessed large numbers of autolysosomes (Fig. 8d,e). By contrast, cells with reduced *Uba1* function had more mitochondria and few autophagic structures (Fig. 8d,f). These data indicate that Uba1 plays an important role in the clearance of cytoplasmic material by regulating autophagy.

DISCUSSION

Autophagy has been shown to influence cell size during growth factor and nutrient restriction in mammalian cells lines [25, 26], but this study indicates that autophagy controls cell size as part of a normal developmental program. Our discovery that *Atg7* and *Atg3* are not required for autophagy and cell size reduction in dying midgut cells in *Drosophila* is surprising. While an *Atg5*-, *Atg7*-, and *LC3*-independent autophagy pathway has been reported [27], we describe autophagy that requires *Atg8/LC3* and does not require *Atg7* and *Atg3*. It has been assumed that components of the core Atg8/LC3 and Atg12 conjugation pathways are used by all eukaryotic cells, but this study provides evidence that alternative factors can function to regulate autophagy in a cell context-specific manner.

This study highlights that autophagy may have different regulatory mechanisms in distinct cell types within an animal. Different forms of autophagy could involve either unique regulatory pathways [28, 29], different amounts/rates of autophagy or alternative cargo selection mechanisms [30], and these are not mutually exclusive. Another possibility is that differences in cargo selection alone, perhaps based on specific cargo adaptor proteins, could mediate a distinct type of autophagy.

We report that an E1 enzyme other than *Atg7* is required for Atg8/LC3 and Atg5 puncta formation, and clearance of p62 and mitochondria. Our studies indicate that *Uba1* fails to function in place of *Atg7*, as expected based on the unique architecture and use of ubiquitin-like proteins and E2 binding domains in these highly divergent E1s [12]. Although we cannot exclude the possibility that Atg8a is activated by unknown factors, the simplest model to explain our data positions *Uba1* function at a different stage of the autophagy process that depends on ubiquitin conjugation. Previous work in a mammalian cell line indicated that *Uba1* is required for protein degradation by lysosomes, but this was not because of decreased autophagosome formation [31]. In addition, recent work in *Drosophila* implicated the de-ubiquitination enzyme USP36 in autophagy [32]. However, the inability of *Atg5* knockdown to suppress the *USP36* mutant phenotype, as well as the accumulation of both GFP-Atg8a and p62 in *USP36* mutant cells, suggests a defect in autophagic flux rather than a defect in the formation of autophagosomes. p62 and other ubiquitin binding proteins are known to facilitate recruitment of ubiquitinated cargoes into autophagosomes [30]. In addition, p62 was recently shown to accumulate at sites of autophagosome formation even when autophagosome formation is blocked [23]. Thus, it is possible that Uba1 promotes cargo recruitment to the sites of autophagosome formation to facilitate autophagy. However, it is also possible that Uba1 could function at multiple stages in the regulation of autophagy.

It is critical to understand the mechanisms that regulate autophagy given the interest in this catabolic process as a therapeutic target for multiple age-associated disorders, including

NIH-PA Author Manuscript

NIH-PA Author Manuscript

NIH-PA Author Manuscript

cancer and neurodegeneration. Significantly, our studies illuminate that autophagy has different regulatory mechanisms in distinct cell types within an animal, and highlight the importance of studying core autophagy genes in specific cell types under physiological conditions.

METHODS

Drosophila strains

We used Canton-S as wild-type control. For loss-of-function mutations (obtained from the Bloomington stock center or otherwise specified), we used *Atg18*^{KG03090}, *Df(3L)*^{6112}, *Atg2*^{EP3697}, *Df(3L)*^{6091}, *Atg1*$^{\Delta 3D}$ [33], *Atg13*$^{\Delta 74}$ [34], *Atg6*^{1} [35], *Vps34*$^{\Delta m22}$ [36], *Atg7*^{d30}, *Atg7*^{d14}, *Atg7*^{d77}, *Atg7*^{d4} [17], *Atg3*^{10} [16], *Atg8a*^{KG07569}, *Df(3L)cat*, and *Uba1*^{H33} [37]. For RNAi knockdown assays, we used *CG7528-1, CG13343-3, CG13343-4* from P. Meier. We used RNAi lines from Vienna Drosophila RNAi Center (VDRC): UAS-*Atg18*^{IR} VDRC Transformant ID (TID) 22646, *UAS-Atg1*^{IR} TID 16133, *UAS-Atg8a*^{IR} TID 43097, UAS-*Atg7*^{IR} TID 45561, UAS-*Atg3*^{IR} TID 108666, *UAS-Uba2*^{IR} TID 110173, *UAS-Aos1*^{IR} TID 47256, *UAS-CG13343*^{IR} TID 105141, *UAS-APP-BP1*^{IR} TID 7728, *UAS-CG13090*^{IR} TID 110326, *UAS-CG13090*^{IR} TID 43558, *UAS-CG1749*^{IR} TID 110395. We also used the following TRiP lines from the Bloomington Stock Center: JF02703 (for *Atg5*) stock number BL27551, HMS01153 (for *Atg12*) BL34675, HMS01347 (for *Atg16*) BL34358, JF01977 (for *Uba1*) BL25957, HM05055 (for *Uba2*) BL28569, HM05183 (for *Aos1*) BL28972, HMS01352 (for *CG1749*) BL34363, and HMS00284 (for *Ub*) BL33405. For mis-expression studies, we used *UAS-p35, UAS-Atg1*^{GS10797} [16], *UAS-mito-GFP* (Bloomington, BL8442, 8443), *UAS-eGFP-Atg5* (BL8731), *UAS-Dts7*^{ts} [18], *UAS-CL1-GFP* [19], and *UAS-Atg4*^{DN} [21].

Induction of cell clones

To induce mis-expression in clones of cells, virgin females of *y w hsFlp*; +; *Act>CD2>GAL4* (> is FRT site), *UAS-DsRed* or *y w hsFlp*; *pmCherry-Atg8a*; *Act>CD2>GAL4, UAS-nlsGFP/TM6B* [38] were crossed to indicated RNAi or transgenic lines. One day egg lays were heat shocked at 37°C except for *Uba1* RNAi clones that were heat shocked at first instar larval stage. To induce loss-of-function clones, we used *y w hsFlp*; +; *FRT80B Ubi-nlsGFP, y w hsFlp*; +; *FRT82B Ubi-GFP, y w hsFlp*; +; *FRT82B Ubi-nlsmRFP, y w hsFlp*; *NP1-GAL4, UAS-mito-GFP*; *FRT80B Ubi-nlsmRFP, y w hsFlp*; *FRT42D Ubi-nlsGFP, y w hsFlp*; *NP1-GAL4, FRT42D Ubi-nlsmRFP*; *UAS-eGFP-Atg5, y w hsFlp*; *NP1-GAL4, FRT42D Ubi-nlsmRFP*; *UAS-mito-GFP, y w hsFlp*; *CG-GAL4, UAS-GFP-Atg8a, FRT42D UAS-myrRFP* [17] and *y w hsFlp, UAS-CD8GFP*; *FRT42D Tub-GAL80*^{ts}; *Tub-GAL4/TM6B*. We heat shocked one day egg lays for 1 hr at 37°C.

Immuno-labeling and microscopy

We dissected midguts in PBS, fixed with 4% formaldehyde in PBS, blocked with 1% bovine serum albumin, and incubated with primary antibodies. We used mouse anti-Discs large (1:100, from Development Studies Hybridoma Bank, Cat#4F3), rat anti-p62 (1:1,000, H. Stenmark), mouse anti-BrC (1: 100, Development Studies Hybridoma Bank, Cat#25E9), guinea pig anti-Hid (1:50, H. D. Ryoo), and mouse anti-ATP synthase complex V (1:1000, Abcam, Cat# ab14748). For secondary antibodies, we used anti-mouse Oregon Green 488, anti-mouse/guinea pig Alexa Fluor 546 antibody (1:250, Invitrogen, Cat#s O-6380, A-11030, and A-11074 respectively), and mounted in VectaShield containing DAPI (Vector Lab, USA) to detect DNA. We imaged samples with a Zeiss Axiophot II microscope. For GFP- or mCherry-Atg8 imaging, we briefly fixed samples with 4% formaldehyde in PBS and stained DNA with Hoechst. DNA is blue in all figures.

NIH-PA Author Manuscript

NIH-PA Author Manuscript

NIH-PA Author Manuscript

Electron microscopy (EM) and immuno-EM

Larval intestines were dissected from control and mutant animals at 2 hours after puparium formation in PBS. Intestines were fixed for 30 minutes at 25°C in 2.5% glutaraldehyde in 0.1 M cacodylate buffer pH 7.4 (Electron Microscopy Sciences), washed 3 times for 5 minutes at 4°C with 0.1M cacodylate buffer pH7.4, post-fixed in buffered 1% osmium tetroxide for 1 hour at room temperature, dehydrated, treated with propylene oxide and infiltrated for embedding in SPI-pon/Araldite.

For immuno-EM, intestines with GFP-positive *Uba1*^{IR} clone cells were dissected at puparium formation, fixed in 3.2% formaldehyde, 0.25% glutaraldehyde, 1% sucrose, 2mM calcium chloride in 0.1M cacodylate buffer pH7.4 at 4°C overnight, buffer washed, dehydrated, infiltrated, and embedded in LR White resin with polymerization for 2 days at 45-50°C. Ultrathin sections on gold grids were subjected to heat-induced antigen retrieval [39], blocked with buffered 1% BSA and 3% powdered milk, incubated with anti-GFP antibody (1:100, Novus Biologicals, Cat# NB 600-308), followed by 18nm colloidal gold donkey anti-rabbit (1:30, Jackson ImmunoResearch, Cat#111-215-144). All ultrathin sections were stained with uranyl acetate and lead citrate before examination using Philips CM10 and FEI Tecnai G2 Bio12 TEMs.

Quantification of cell size

All control and mutant midguts were processed in an identical fashion for image acquisition. Two-dimensional (2D) cell size was quantified using the measure outline function of Zeiss Axiovision Rel 4.7 software (Zeiss Inc, USA). Three-dimensional (3D) images were acquired using the Z-stack function of Zeiss Axiovision software, and quantified using Volocity software (Perkin Elmer, USA). We compared the 2D and 3D measurements of control and mutant midgut cells at both the third larval instar and white pre-pupal stages (Figure 2), and determined that 2D measurements of cell size accurately reflect 3D measurements. Therefore, we used 2D measurements of cell size in all additional experiments. The number (n) analyzed in each experiment represents number of intestines analyzed, and 1-5 cells of each genotype were measured/intestine.

Starvation of larvae

Early third instar larvae were transferred from food to 20% sucrose in PBS for 4 h.

Quantification of mitochondria number

Mitochondria numbers were quantified from 2 distinct 25 μm^2 regions per cell from 2 cells per animal and at least 3 individual animals/genotype.

Immuno-blotting

Midguts were dissected in PBS at puparium formation. Proteins were extracted with RIPA buffer with complete protease inhibitor (Roche). Western blotting was performed using rabbit anti-Atg8 (1:500, S. Cherry), mouse anti-β-Tubulin (1:50, Development Studies Hybridoma Bank, Cat# E7), HRP-conjugated goat anti-rabbit and anti-mouse IgG (1:2000, Invitrogen, Cat# G-21234 and G-21040 respectively) as previously described [40]. Three independent biological experiments were performed.

Protein production and E1 activating enzyme charging assay

Open reading frames for *Drosophila* Uba1, Atg7, and Atg8a were cloned into pDONR223 using the Gateway recombination system (Invitrogen). Expression constructs were also constructed using Gateway recombination. Recombinant FLAG-tagged Uba1 and Atg7 were produced in Sf9 cells using the Bac-N-Blue system (Invitrogen). Cells were lysed using 50

NIH-PA Author Manuscript

NIH-PA Author Manuscript

NIH-PA Author Manuscript

mM Tris-HCl pH 7.5, 150 mM NaCl, 0.5% NP40, 1 mM DTT, and EDTA-free protease inhibitor cocktail (Roche) and then ruptured using a dounce homogenizer. Lysates were precleared by spinning in a table-top centrifuge at 16,000 × g at 4°C for 20 minutes and the FLAG-tagged proteins were purified using anti-FLAG M2 affinity gel (Sigma). Proteins were eluted using 3× FLAG peptide (Sigma). The buffer was exchanged and the FLAG peptide removed by spinning the eluate in an Ultracel 10K Amicon Ultra centrifugal unit (Millipore) and finally stored in a buffer containing 50 mM Tris-HCl pH 7.5, 150 mM NaCl, 1mM DTT, and 10% glycerol. Recombinant His-Thioredoxin-tagged Atg8a was produced using the pET59-DEST vector (EMD Millipore) and expressed in Rosetta DE3 cells (EMD Millipore). Following induction with 0.4 mM IPTG for 4 hours at 37°C, Atg8a was purified using Ni-NTA agarose (Qiagen) and stored in 50 mM Tris-HCl pH 7.5, 150 mM NaCl, 1 mM DTT, and 10% glycerol. Recombinant human ubiquitin was purchased from Boston Biochem.

Charging reactions were set up on ice in a buffer containing 50 mM Tris-HCl pH 7.5, 5 mM KCl, 5 mM $MgCl_2$, and 1mM DTT made up to a total of 30 μL. For each reaction 10 nM E1, 500 nM ubiquitin, or 500 nM HIS-Atg8a were added where appropriate. Just before starting the reaction, ATP was added to 2 mM final concentration and the reactions were performed at 30°C for 15 minutes. Immediately following the reaction, samples were incubated with 2× Laemmli sample buffer with either 50 mM MES pH5.0 or 10% v/v β-Mercaptoethanol as indicated. Samples were incubated at room temperature and loaded onto two 4-12% NuPAGE Bis-Tris gels (Invitrogen), run in MES running buffer (Invitrogen). Gels were processed for immunoblotting with either rabbit anti-His H-15 (Santa Cruz, Cat#sc-803), mouse anti-Flag M2 (Sigma, Cat#F3165), or rabbit anti-Ubiquitin (Dako, Cat# Z0458) antibodies at 1:1000 in 5% milk in TBS plus 10% Tween-20 (Sigma). Two independent experiments were performed.

Statistics

Indicated *P* values were obtained using a two-tailed t-test, and all quantitative data are shown as mean ± standard deviation.

Supplementary Material

Refer to Web version on PubMed Central for supplementary material.

Acknowledgments

We thank A. Bergmann, M. Brodsky, S. Cherry, G. Juhasz, P. Meier, T.P. Neufeld, H. Stenmark, the Bloomington Stock Center, the VDRC, and the Developmental Studies Hybridoma Bank for flies and antibodies, G. Juhasz for advice about immuno-EM, and T. Fortier for technical support, M. Freeman, S. Doxsey and the Baehrecke lab for constructive comments. This work was supported by NIH grants GM079431 to EHB, GM095567 to JWH, and S10RR027897 to the UMass EM Core, and by Millennium Pharamceuticals to JWH. EHB is an Ellison Medical Foundation Scholar and a member of the UMass DERC (DK32520).

REFERENCES

1. Mizushima N, Komatsu M. Autophagy: Renovation of Cells and Tissues. Cell. 2011; 147:728–741. [PubMed: 22078875]
2. Levine B, Yuan J. Autophagy in cell death: an innocent convict? J. Clin. Invest. 2005; 115:2679–2688. [PubMed: 16200202]
3. Baehrecke EH. Autophagy: dual roles in life and death? Nature Reviews Mol. Cell Biol. 2005; 6:505–510.
4. Berry DL, Baehrecke EH. Growth arrest and autophagy are required for salivary gland cell degradation in Drosophila. Cell. 2007; 131:1137–1148. [PubMed: 18083103]

NIH-PA Author Manuscript

NIH-PA Author Manuscript

NIH-PA Author Manuscript

5. Hou YC, Chittaranjan S, Barbosa SG, McCall K, Gorski SM. Effector caspase Dcp-1 and IAP protein Bruce regulate starvation-induced autophagy during Drosophila melanogaster oogenesis. J. Cell Biol. 2008; 182:1127–1139. [PubMed: 18794330]
6. Nezis IP, et al. Autophagic degradation of dBruce controls DNA fragmentation in nurse cells during late Drosophila melanogaster oogenesis. J. Cell Biol. 2010; 190:523–531. [PubMed: 20713604]
7. Mizushima N, Levine B, Cuervo AM, Klionsky DJ. Autophagy fights disease through cellular self-digestion. Nature. 2008; 451:1069–1075. [PubMed: 18305538]
8. Tsukada M, Ohsumi Y. Isolation and characterization of autophagy-defective mutants of Saccharomyces cerevisiae. FEBS Lett. 1993; 333:169–174. [PubMed: 8224160]
9. Thumm M, et al. Isolation of autophagocytosis mutants of Saccharomyces cerevisiae. FEBS Lett. 1994; 349:275–280. [PubMed: 8050581]
10. Harding TM, Morano KA, Scott SV, Klionsky DJ. Isolation and characterization of yeast mutants in the cytoplasm to vacuole protein targeting pathway. J. Cell Bio. 1995; 131:591–602. [PubMed: 7593182]
11. Harding TM, Hefner-Gravink A, Thumm M, Klionsky DJ. Genetic and phenotypic overlap between autophagy and the cytoplasm to vacuole protein. J. Biol. Chem. 1996; 271:17621–17624. [PubMed: 8663607]
12. Schulman BA, Harper JW. Ubiquitin-like protein activation by E1 enzymes: the apex for downstream signalling pathways. Nat. Rev. Mol. Cell Biol. 2009; 10:319–331. [PubMed: 19352404]
13. Denton D, et al. Autophagy, not apoptosis, is essential for midgut cell death in Drosophila. Curr. Biol. 2009; 19:1741–1746. [PubMed: 19818615]
14. Lee C-Y, Cooksey BAK, Baehrecke EH. Steroid regulation of midgut cell death during Drosophila development. Dev. Biol. 2002; 250:101–111. [PubMed: 12297099]
15. Micchelli CA, Sudmeier L, Perrimon N, Tang S, Evans R. Identification of adult midgut precursors in Drosophila. Gene Expr. Patterns. 2011; 11:12–21. [PubMed: 20804858]
16. Scott RC, Juhász G, Neufeld TP. Direct induction of autophagy by Atg1 inhibits cell growth and induces apoptotic cell death. Curr. Biol. 2007; 17:1–11. [PubMed: 17208179]
17. Juhász G, Erdi B, Sass M, Neufeld TP. Atg7-dependent autophagy promotes neuronal health, stress tolerance, and longevity but is dispensable for metamorphosis in Drosophila. Genes Dev. 2007; 21:3061–3066. [PubMed: 18056421]
18. Belote JM, Fortier E. Targeted expression of dominant negative proteasome mutants in Drosophila melanogaster. Genesis. 2002; 34:80–82. [PubMed: 12324954]
19. Pandey UB, et al. HDAC6 rescues neurodegeneration and provides an essential link between autophagy and the UPS. Nature. 2007; 447:859–863. [PubMed: 17568747]
20. Fujita N, et al. An Atg4B mutant hampers the lipidation of LC3 paralogues and causes defects in autophagosome closure. Mol. Biol. Cell. 2008; 19:4651–4659. [PubMed: 18768752]
21. Pircs K, et al. Advantages and Limitations of Different p62-Based Assays for Estimating Autophagic Activity in Drosophila. PLoS ONE. 2012; 7:e44214. [PubMed: 22952930]
22. Jiang C, Baehrecke EH, Thummel CS. Steroid regulated programmed cell death during Drosophila metamorphosis. Development. 1997; 124:4673–4683. [PubMed: 9409683]
23. Itakura E, Mizushima N. p62 targeting to the autophagosome formation site requires self-oligomerization but not LC3 binding. J. Cell Biol. 2011; 192:17–27. [PubMed: 21220506]
24. Fujita K, Maeda D, Xiao Q, Srinivasula SM. Nrf2-mediated induction of p62 controls Toll-like receptor-4-driven aggresome-like induced structure formation and autophagic degradation. Proc. Natl. Acad. Sci. U S A. 2011; 108:1427–1432. [PubMed: 21220332]
25. Lum JJ, et al. Growth factor regulation of autophagy and cell survival in the absence of apoptosis. Cell. 2005; 120:237–248. [PubMed: 15680329]
26. Hosokawa N, Hara Y, Mizushima N. Generation of cell lines with tetracycline-regulated autophagy and a role for autophagy in controlling cell size. FEBS Lett. 2006; 580:2623–2629. [PubMed: 16647067]
27. Nishida Y, et al. Discovery of Atg5/Atg7-independent alternative macroautophagy. Nature. 2009; 461:654–658. [PubMed: 19794493]

NIH-PA Author Manuscript

NIH-PA Author Manuscript

NIH-PA Author Manuscript

28. Tian Y, et al. C. elegans screen identifies autophagy genes specific to multicellular organisms. Cell. 2010; 141:1042–1055. [PubMed: 20550938]
29. McPhee CK, Logan MA, Freeman MR, E H, B. Activation of autophagy during cell death requires the engulfment receptor Draper. Nature. 2010; 465:1093–1096. [PubMed: 20577216]
30. Johansen T, Lamark T. Selective autophagy mediated by autophagic adapter proteins. Autophagy. 2011; 7:279–296. [PubMed: 21189453]
31. Lenk SE, Dunn WAJ, Trausch JS, Ciechanover A, Schwartz AL. Ubiquitin-activating enzyme, E1, is associated with maturation of autophagic vacuoles. J. Cell Biol. 1992; 118:301–308. [PubMed: 1321157]
32. Taillebourg E, et al. The deubiquitinating enzyme USP36 controls selective autophagy activation by ubiquitinated proteins. Autophagy. 2012; 8:767–779. [PubMed: 22622177]
33. Scott RC, Schuldiner O, Neufeld TP. Role and regulation of starvation-induced autophagy in the Drosophila fat body. Dev. Cell. 2004; 7:167–178. [PubMed: 15296714]
34. Chang YY, Neufeld TP. An Atg1/Atg13 complex with multiple roles in TOR-mediated autophagy regulation. Mol. Biol. Cell. 2009; 20:2004–2014. [PubMed: 19225150]
35. Shravage BV, Hill JH, Powers CM, Wu L, Baehrecke EH. Atg6 is required for multiple vesicle trafficking pathways and hematopoiesis in Drosophila. Development. 2013; 140:1321–1329. [PubMed: 23406899]
36. Juhász G, et al. The class III PI(3)K Vps34 promotes autophagy and endocytosis but not TOR signaling in Drosophila. J. Cell Biol. 2008; 181:2347–2360.
37. Lee TV, et al. The E1 ubiquitin-activating enzyme Uba1 in Drosophila controls apoptosis autonomously and tissue growth non-autonomously. Development. 2008; 135:43–52. [PubMed: 18045837]
38. Denton D, et al. Relationship between growth arrest and autophagy in midgut programmed cell death in Drosophila. Cell Death Differ. 2012; 19:1299–1307. [PubMed: 22555456]
39. Yamashita S. The post-embedding method for immunoelectron microscopy of mammalian tissues: a standardized procedure based on heat-induced antigen retrieval. Methods Mol. Biol. 2010; 657:237–248. [PubMed: 20602221]
40. Dutta S, Baehrecke EH. Warts is required for PI3K-regulated growth arrest, autophagy, and autophagic cell death in Drosophila. Curr. Biol. 2008; 18:1466–1475. [PubMed: 18818081]

NIH-PA Author Manuscript
NIH-PA Author Manuscript
NIH-PA Author Manuscript

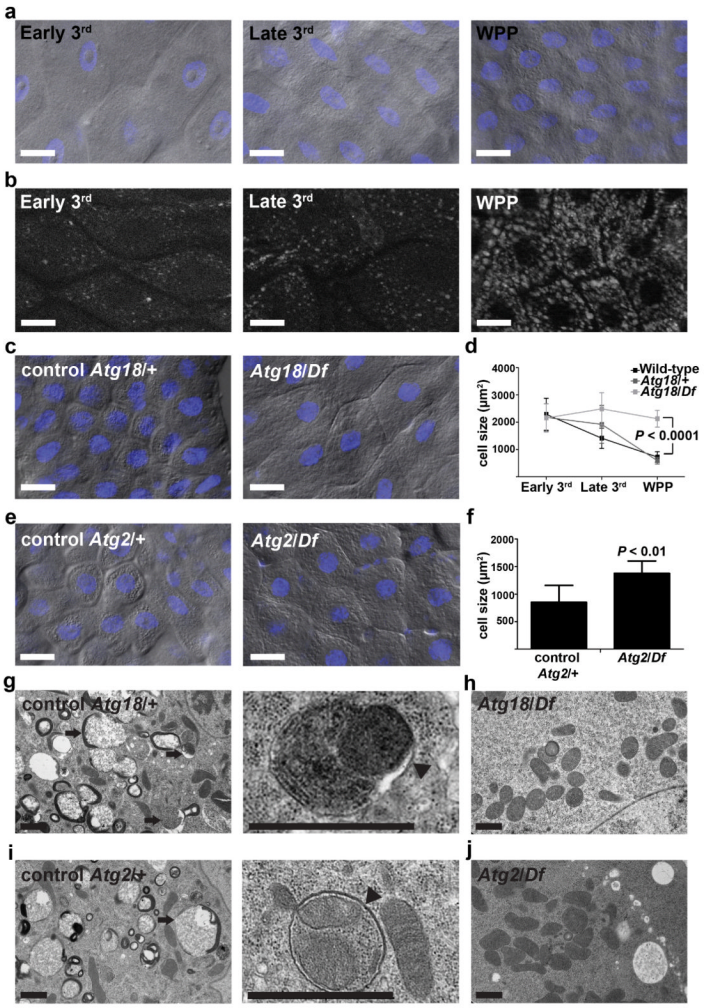

Figure 1.

Atg18 and *Atg2* are required for programmed cell size reduction in the *Drosophila* midgut. (**a**) Representative differential interference contrast (DIC) microscopy images of midgut cells from wild-type animals at the early third instar larval (Early 3rd), late third instar larval (Late 3rd) and at puparium formation (white prepupal, WPP) stages. (**b**) Autophagy detected by formation of mCherry-Atg8a punctate spots in midgut cells from wild-type animals at indicated stages. Representative images are shown. (**c**) Midguts from control $Atg18^{KG03090}$/wild-type (*Atg18*/+), n =14, and $Atg18^{KG03090}/Df(3L)^{6112}$ mutant (*Atg18/Df*), n = 11, animals at puparium formation analyzed by DIC microscopy. Representative images are shown. (**d**) Wild-type, control ($Atg18^{KG03090}$/+) and *Atg18* mutant (*Atg18/Df*) midgut cell size quantification (μm^2) at indicated stages, n = 10 animal intestines/genotype with 5 cells measured/intestine/stage. (**e**) DIC images of midgut cells from $Atg2^{EP3697}$/wild-type control (*Atg2*/+) and $Atg2^{EP3697}/Df(3L)^{6091}$ mutant (*Atg2/Df*) animals at puparium formation. Representative images are shown. (**f**) Cell size quantification (μm^2) from **e**, n = 12 (*Atg2*/+) and n = 7 (*Atg2/Df*) animal intestines/genotype with 5 cells measured/intestine. (**g**-**j**) Representative TEM images of intestine cells 2 hours after puparium formation. (**g**,**i**) Control $Atg18^{KG03090}$/wild-type (*Atg18*/+, **g**) and $Atg2^{EP3697}$/wild-type control (*Atg2*/+, **i**) cells with an enlarged image showing a double membrane structure (arrowhead) that surrounds a mitochondrion and endoplasmic reticulum. Arrows indicate autolysosomes. (**h**,**j**) $Atg18^{KG03090}/Df(3L)^{6112}$ mutant (*Atg18/Df*, **h**) cell and $Atg2^{EP3697}/Df$ (*Atg2/Df*, **j**)

mutant cells lacking autophagic structures. Quantification is shown as mean ± standard deviation (s.d.). Scale bars represent 20 μm (**a-c** and **e**) and 1 μm (**g-j**).

NIH-PA Author Manuscript
NIH-PA Author Manuscript
NIH-PA Author Manuscript

NIH-PA Author Manuscript
NIH-PA Author Manuscript
NIH-PA Author Manuscript

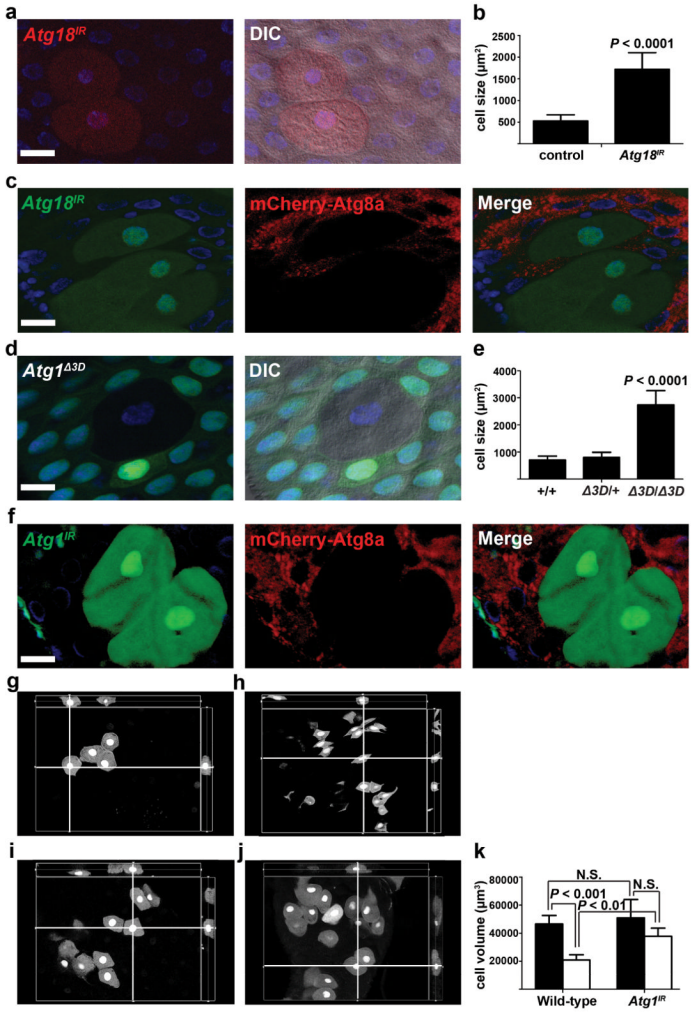

Figure 2.

Programmed size reduction is cell autonomous and requires *Atg18* and *Atg1*. (**a**) Midguts dissected from animals expressing $Atg18^{IR}$ specifically in DsRed-marked clones of cells at puparium formation and analyzed by fluorescence and DIC microscopy. Representative images are shown. (**b**) Quantification (μm^2) from **a**, $n = 12$ animal intestines/genotype with 1-5 cells measured/intestine. (**c**) Midguts expressing mCherry-Atg8a in all cells, and expressing $Atg18^{IR}$ specifically in GFP-marked cell clones dissected from animals at 2 h after puparium formation. Representative images are shown. (**d**) Midguts dissected from animals at puparium formation that contain an $Atg1^{\Delta 3D}$ loss-of-function mutant cell clone (lacking GFP) and analyzed by fluorescence and DIC microscopy. Wild-type (+/+) control cell possesses stronger GFP and heterozygous $Atg1^{\Delta 3D}$/wild-type ($\Delta 3D$/+) cells have weaker GFP. Representative images are shown. (**e**) Quantification (μm^2) from **d**, $n = 7$ (+/+), $n = 8$ ($\Delta 3D$/+), and $n = 8$ ($\Delta 3D/\Delta 3D$) animal intestines/genotype with 1-5 cells measured/intestine. (**f**) Midguts dissected from animals expressing mCherry-Atg8a in all cells, and expressing $Atg1^{IR}$ specifically in GFP-marked clones of cells at 2 h after puparium formation. Representative images are shown. (**g-j**) Representative cut views from 3D reconstitution images from wild-type (**g**,**h**) and *Atg1* knockdown (**i**,**j**) cells at early 3rd instar larval stage (**g**,**i**) and at puparium formation (**h**,**j**). (**k**) Quantification of cell volume (μm^3) from **g-j**, $n = 5$ animal intestines/genotype with 1-5 cells measured/intestine/stage.

Black columns: early 3rd instar larval stage. White columns: puparium formation stage. Quantification is shown as mean ± s.d.. N.S.: no significance. Scale bars represent 20 μm.

NIH-PA Author Manuscript
NIH-PA Author Manuscript
NIH-PA Author Manuscript

NIH-PA Author Manuscript

NIH-PA Author Manuscript

NIH-PA Author Manuscript

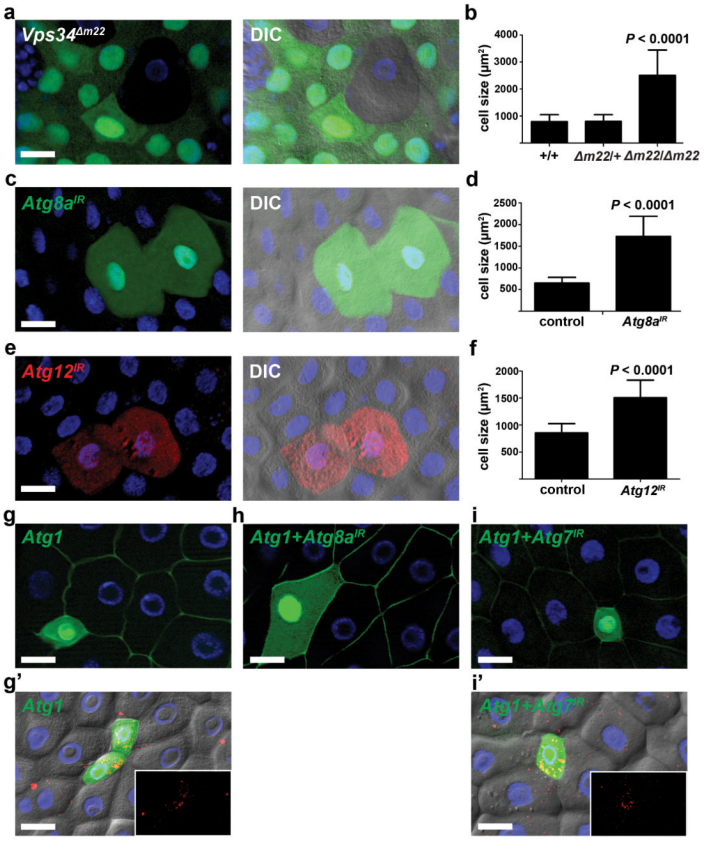

Figure 3.

Autophagy is necessary and sufficient for cell size reduction. (**a**) Midguts dissected from animals at puparium formation that contain *Vps34*$^{\Delta m22}$ loss-of-function mutant cell clones (lacking GFP) and analyzed by fluorescence and DIC microscopy. Wild-type (+/+) control cells possess stronger GFP and heterozygous *Vps34*$^{\Delta m22}$/wild-type (*Δm22*/+) cells have weaker GFP. Representative images are shown. (**b**) Quantification (μm^2) from **a**, *n* = 14 animal intestines/genotype with 1-5 cells measured/intestine. (**c**) Midguts dissected from animals expressing *Atg8a*^{IR} specifically in GFP-marked clones of cells at puparium formation and analyzed by fluorescence and DIC microscopy. Representative images are shown. (**d**) Cell size quantification (μm^2) from **c**, *n* = 10 animal intestines/genotype with 1-5 cells measured/intestine. (**e**) Midguts dissected from animals expressing *Atg12*^{IR} specifically in DsRed-marked clones of cells at puparium formation and analyzed by fluorescence and DIC microscopy. Representative images are shown. (**f**) Cell size quantification (μm^2) from **e**, *n* = 14 animal intestines/genotype with 1-5 cells measured/intestine. (**g-i**) Midguts dissected from early third instar larvae that mis-express *Atg1*^{GS10797} (*Atg1*) (**g**, GFP in nucleus and cytoplasm), both *Atg1* + *Atg8a*^{IR} (**h**), or both *Atg1* + *Atg7*^{IR} (**i**) and stained to detect Discs large (green) on the cortex of all cells. Representative images are shown. (**g**' and **i**') DIC images of midguts expressing mCherry-Atg8a in all cells, *Atg1* (**g**'), and *Atg1* + *Atg7*^{IR} (**i**') in GFP-marked clones of cells. mCherry-Atg8a puncta are shown in insets. Representative images are shown. Quantification is shown as mean ± s.d.. Scale bars represent 20 μm.

NIH-PA Author Manuscript
NIH-PA Author Manuscript
NIH-PA Author Manuscript

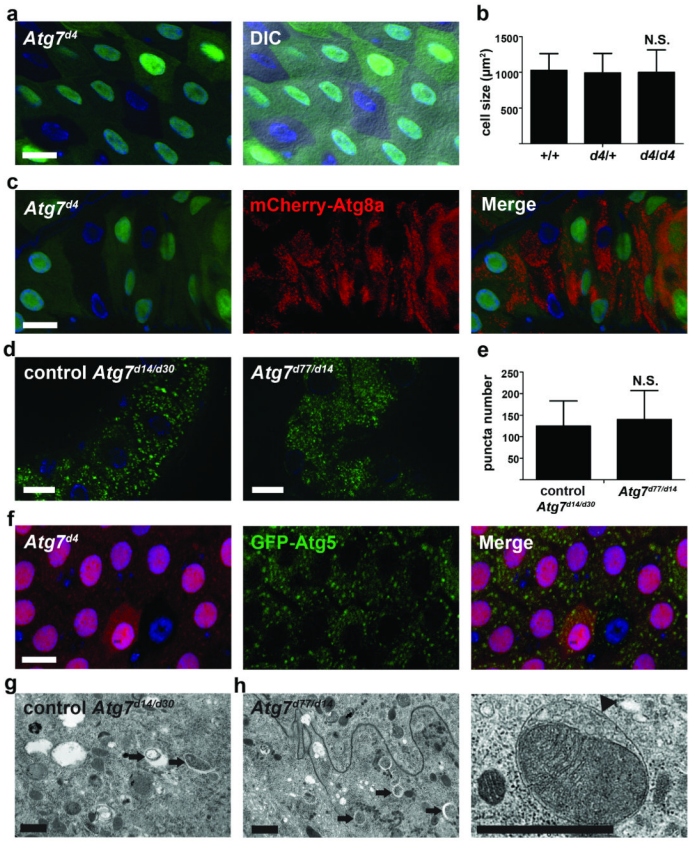

Figure 4.

Atg7 is not required for programmed cell size reduction and autophagy. (**a**) Midguts dissected from animals at puparium formation that contain $Atg7^{d4}$ loss-of-function mutant cell clones (lacking GFP) and analyzed by fluorescence and DIC microscopy. Wild-type (+/+) control cells possess stronger GFP and heterozygous $Atg7^{d4}$/wild-type (*d4*/+) cells have weaker GFP. Representative images are shown. (**b**) Cell size quantification (μm^2) from **a**, *n* = 8 animal intestines/genotype with 1-5 cells measured/intestine. (**c**) Midguts expressing mCherry-Atg8a in all cells, and with $Atg7^{d4}$ loss-of-function clone cells (lacking GFP) at 2h after puparium formation. Representative images are shown. (**d**) Gastric caeca expressing GFP-Atg8a in all cells from control ($Atg7^{d30/d14}$) and *Atg7* mutant ($Atg7^{d77/d14}$) animals. Representative images are shown. (**e**) Quantification of GFP-Atg8a puncta number from **d**, *n* = 31 animal intestines/genotype with puncta quantified in image field/intestine. (**f**) Midguts expressing GFP-Atg5 in in enterocytes (larger nuclei) with an $Atg7^{d4}$ loss-of-function clone cell (lacking RFP) at puparium formation. Representative images are shown. (**g**,**h**) Representative TEM images of intestine cells 2 h after puparium formation. Arrows indicate autolysosomes. (**g**) Control ($Atg7^{d30/d14}$) and (**h**) *Atg7* mutant ($Atg7^{d77/d14}$) cells both contain autophagic structures. (**h**) Enlarged *Atg7* mutant cell image of a double membrane autophagosome (arrowhead) surrounding a mitochondrion. Quantification is shown as mean ± s.d.. N.S.: no significance. Scale bars represent 20 μm (**a**,**c**,**d**, and **f**) and 1 μm (**g**,**h**).

NIH-PA Author Manuscript

NIH-PA Author Manuscript

NIH-PA Author Manuscript

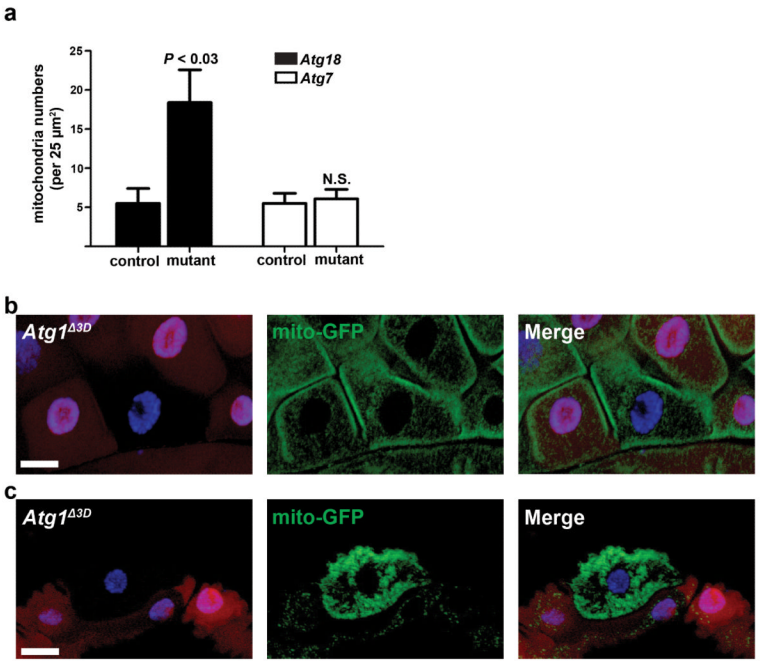

Figure 5.

Autophagy is required for clearance of mitochondria. (**a**) Quantification of mitochondria numbers from *Atg18* control (*Atg18*^{KG03090}/wild-type) and mutant (*Atg18*^{KG03090}/*Df(3L)*^{6112}) or *Atg7* control (*Atg7*$^{d30/d14}$) and mutant (*Atg7*$^{d77/d14}$) TEM images. Mitochondria were quantified from 2 distinct 25 μm^2 regions per cell from 2 cells per animal from at least 3 different animals/genotype. (**b, c**) Midguts dissected from either early third instar larvae (**b**) or at puparium formation (**c**) that express GFP-labeled mitochondria in all cells and contain an *Atg1*$^{\Delta 3D}$ loss-of-function mutant cell clone (lacking RFP). Wild-type control cells possess stronger RFP and heterozygous cells have weaker RFP. Representative images are shown. Quantification is shown as mean ± s.d.. N.S.: no significance. Scale bars represent 20 μm.

NIH-PA Author Manuscript
NIH-PA Author Manuscript
NIH-PA Author Manuscript

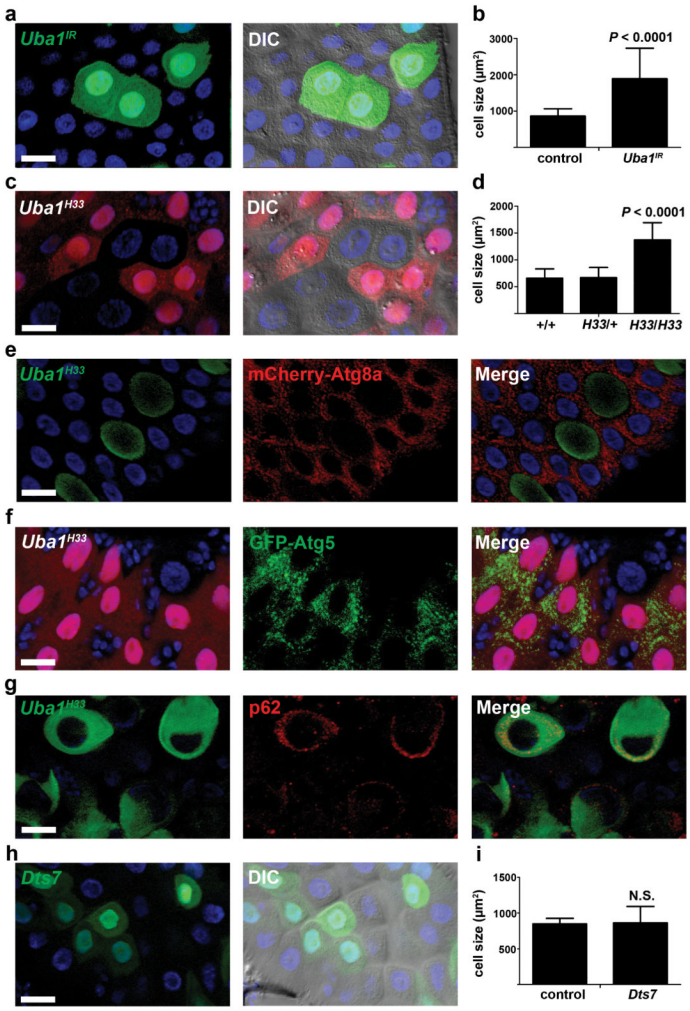

Figure 6.

Uba1 is required for midgut cell programmed size reduction and autophagy. (**a**) Midguts dissected from animals expressing $Uba1^{IR}$ specifically in GFP-marked clones of cells at puparium formation and analyzed by fluorescence and DIC microscopy. Representative images are shown. (**b**) Cell size quantification (μm^2) from **a**, $n = 16$ animal intestines/genotype with 1-5 cells measured/intestine. (**c**) Midguts dissected from animals at puparium formation that contain $Uba1^{H33}$ loss-of-function mutant cell clones (lacking RFP) and analyzed by fluorescence and DIC microscopy. Wild-type (+/+) control cells possess stronger RFP and heterozygous $Uba1^{H33}$/wild-type (*H33*/+) cells have weaker RFP. Representative images are shown. (**d**) Quantification (μm^2) from **c**, $n = 8$ (+/+), $n = 11$ (*H33*/+), and $n = 11$ (*H33/H33*) animal intestines/genotype with 1-5 cells measured/intestine. (**e**) Midguts dissected from animals at puparium formation that contain $Uba1^{H33}$ loss-of-function MARCM mutant cell clones (GFP-positive) that also have mCherry-Atg8a expressed in all cells and analyzed by fluorescence microscopy. Control wild-type and heterozygous cells have no GFP. Representative images are shown. (**f**) Midguts expressing GFP-Atg5 in enterocytes (larger nuclei), and with an $Uba1^{H33}$ loss-of-function clone cell (lacking RFP) at puparium formation analyzed by fluorescence microscopy. Representative images are shown. (**g**) Midguts dissected from animals at puparium formation that contain $Uba1^{H33}$ loss-of-function MARCM mutant cell clones (GFP-positive) that are stained with

NIH-PA Author Manuscript

NIH-PA Author Manuscript

NIH-PA Author Manuscript

p62 antibody and analyzed by fluorescence microscopy. Control wild-type and heterozygous cells have no GFP. Representative images are shown. (**h**) Midguts dissected from animals expressing *Dts7*, a dominant temperature sensitive mutant of the β2 subunit of the proteasome, specifically in GFP-marked cells at puparium formation and analyzed by fluorescence and DIC microscopy. Representative images are shown. (**i**) Cell size quantification (μm^2) from **h**, $n = 6$ animal intestines/genotype with 1-5 cells measured/intestine. Quantification is shown as mean ± s.d.. N.S.: no significance. Scale bars represent 20 μm.

NIH-PA Author Manuscript

NIH-PA Author Manuscript

NIH-PA Author Manuscript

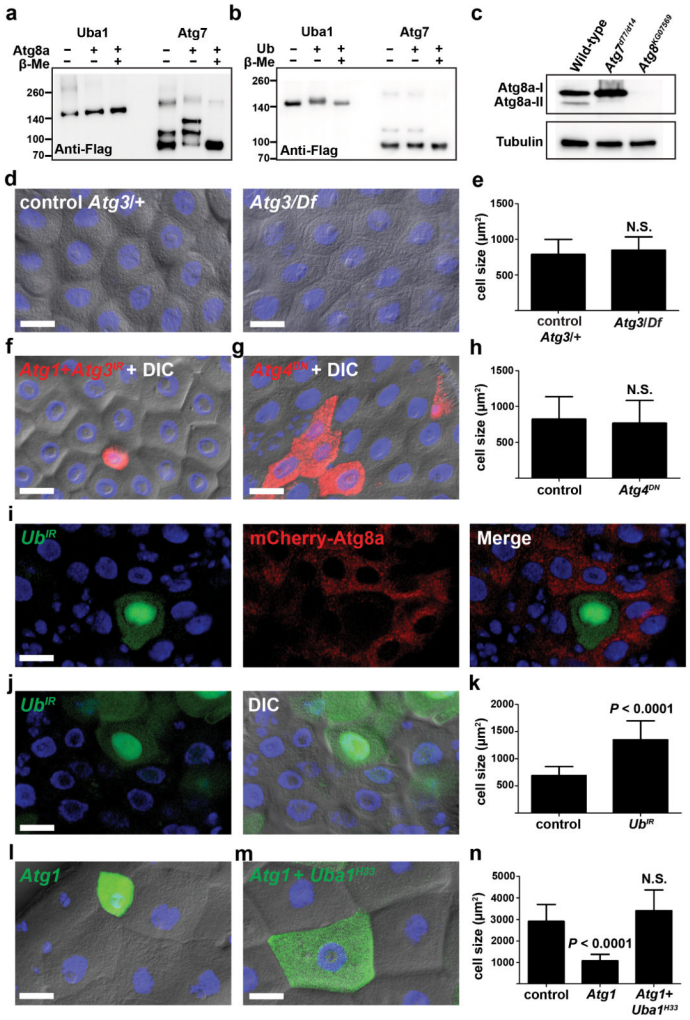

Figure 7.

Role of *Uba1* in midgut autophagy. (**a** and **b**) E1 charging assay for Uba1 and Atg7 with either Atg8a (**a**) or Ub (**b**), $n = 2$ experiments with independently isolated proteins and analyses. Flag-tagged baculoviral expressed E1s were incubated with either His-tagged Atg8a or Ub in the presence or absence of β-mercaptoethanol, separated by electrophoresis and blotted. Band shift was detected with anti-Flag antibody. Molecular weight ladders are indicated. Representative images are shown. Molecular weights: Flag-Uba1 135 kDa, Flag-Atg7 81 kDa, His-Atg8a 29kDa, Ub 9 kDa. (**c**) Midgut protein extracts at puparium formation from wild-type, *Atg7* mutant ($Atg7^{d77/d14}$) and *Atg8* ($Atg8^{KG07569}$) mutant blotted with anti-Atg8 and anti-Tubulin, $n = 3$ independent biological experiments. Representative images are shown. (**d**) Midguts from control $Atg3^{10}$/wild-type (*Atg3*/+), and $Atg3^{10}$*/Df(3L)cat* mutant (*Atg3/Df*) animals at puparium formation analyzed by DIC microscopy. Representative images are shown. (**e**) Cell size quantification (μm^2) from **d**, $n = 11$ (*Atg3*/+) and $n = 9$ (*Atg3/Df*) animal intestines/genotype with 5 cells measured/intestine. (**f**) Midguts dissected from early 3rd instar larvae that mis-express $Atg1^{GS10797}$ (*Atg1*) and $Atg3^{IR}$ only in the DsRed-marked cell clone and analyzed by fluorescence and DIC microscopy. Representative images are shown. (**g**) Midguts dissected from animals expressing $Atg4^{DN}$ specifically in DsRed-marked clones of cells at puparium formation and analyzed by fluorescence and DIC microscopy. Representative images are shown. (**h**) Cell

NIH-PA Author Manuscript

NIH-PA Author Manuscript

NIH-PA Author Manuscript

size quantification (μm^2) from **g**, n = 10 animal intestines/genotype with 1-5 cells measured/intestine. (**i**) Midguts dissected from animals expressing mCherry-Atg8a in all cells, and expressing Ub^{IR} specifically in GFP-marked clones of cells at puparium formation. Representative images are shown. (**j**) Midguts dissected from animals expressing Ub^{IR} specifically in GFP-marked clones of cells at puparium formation and analyzed by fluorescence and DIC microscopy. Representative images are shown. (**k**) Cell size quantification (μm^2) from **j**, n = 12 animal intestines/genotype with 1-5 cells measured/intestine. (**l**,**m**) Midguts dissected from early third instar larvae that contain $Atg1^{GS10797}$ (*Atg1*) mis-expression in either a wild-type GFP positive cell clone (**l**) or a $Uba1^{H33}$ loss-of-function MARCM mutant cell clone (GFP-positive) (**m**) and analyzed by fluorescence and DIC microscopy. Control wild-type and heterozygous $Uba1^{H33}$/wild-type cells have no GFP. Representative images are shown. (**n**) Quantification (μm^2) from **l** and **m**, n = 22 (control), n = 16 (*Atg1*), and n =6 (*Atg1* + $Uba1^{H33}$) animal intestines/genotype with 1-5 cells measured/intestine. Quantification of control cells (**l**,**m**) were pooled since they are genetically identical. Quantification is shown as mean ± s.d.. N.S.: no significance. Scale bars represent 20 μm.

NIH-PA Author Manuscript
NIH-PA Author Manuscript
NIH-PA Author Manuscript

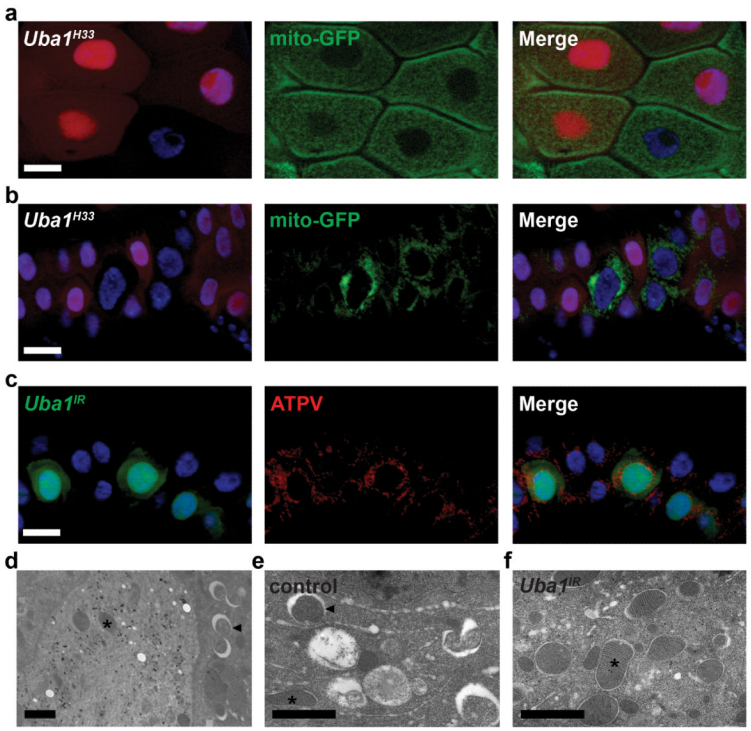

Figure 8.

Uba1 is required for clearance of mitochondria. (**a, b**) Midguts dissected from either early third instar larvae (**a**) or at puparium formation (**b**) that express GFP-labeled mitochondria in enterocytes (larger nuclei) and contain $Uba1^{H33}$ loss-of-function mutant cell clones (lacking RFP). Wild-type control cells possess stronger RFP and heterozygous cells have weaker RFP. Representative images are shown. (**c**) Midguts dissected at puparium formation that express $Uba1^{IR}$ (GFP in nucleus and cytoplasm) and stained with ATP synthase complex V (ATPV) to detect mitochondria in all cells. Representative images are shown. (**d-f**) Representative immuno-TEM images of $Uba1^{IR}$ clone cells at puparium formation. $Uba1^{IR}$-expressing cells possess gold particles, while control cells lack gold particles (**d**). Control cells possess numerous autolysosomes in the cytoplasm (arrowheads) and few mitochondria (asterisks), while $Uba1^{IR}$-expressing cells possess numerous mitochondria and few autophagic structures. Scale bars represent 20 μm (**a-c**) and 1 μm (**d-f**).